

## RESEARCH ARTICLE

# Time course of dorsolateral geniculate nucleus plasticity in adult monkeys with laser-induced retinal lesions

Sandra S. Pereira<sup>1,2</sup> | Eliã P. Botelho<sup>1</sup> | Juliana G.M. Soares<sup>1</sup> | Mariana F. Farias<sup>1</sup> | Ricardo Gattass<sup>1</sup> 

<sup>1</sup>Laboratory of Cognitive Physiology, Instituto de Biofísica Carlos Chagas Filho, UFRJ, Rio de Janeiro, RJ, Brazil

<sup>2</sup>Department of Ophthalmology, School of Medicine, UFRJ, Rio de Janeiro, RJ, Brazil

## Correspondence

Prof. Dr. Ricardo Gattass, Instituto de Biofísica Carlos Chagas Filho, Bloco G, CCS, Rio de Janeiro, RJ, 21941 - Brasil.  
Email: [rgattass@gmail.com](mailto:rgattass@gmail.com)

## Funding information

Fundação Carlos Chagas Filho de Amparo à Pesquisa do Estado do Rio de Janeiro, Grant/Award Numbers: E-26/110.192/2013, E-26/110.905/2013; Financiadora de Estudos e Projetos, Grant/Award Number: 0354/16

## Abstract

We studied changes in the expression of growth-associated protein 43 (GAP43), glial fibrillary acidic protein (GFAP), and calcium-binding proteins (calbindin [Cb] and parvalbumin [Pv]) in the dorsal lateral geniculate nucleus (dLGN) of four capuchin monkeys with laser-induced retinal lesions. The lesions were generated with the aid of a neodymium-YAG dual-frequency laser with shots of different intensity and at different survival time in each animal. The expression of these proteins in the layers of the dLGN was evaluated by performing histodensitometry of coronal sections throughout the nucleus. High-power laser shots administered at the border of the optic disc (OD)-injured fibers resulted in large scotomas. These lesions produced a devastating effect on fibers in this passage, resulting in large deafferentation of the dLGN. The time course of plasticity expressed in this nucleus varied with the degree of the retinal lesion. Topographically, corresponding portions of the dLGN were inferred by the extent of the ocular dominance column revealed by cytochrome oxidase histochemistry in flattened preparations of V1. In the region representing the retinal lesion, the expression of GFAP, GAP43, Pv, and Cb increased and decreased in the corresponding dLGN layers shortly after lesion induction and returned to their original values with different time courses. Synaptogenesis (indicated by GAP43 expression) appeared to be increased in all layers, while “cleansing” of the glial-damaged region (indicated by GFAP expression) was markedly greater in the parvocellular layers, followed by the magnocellular layers.

Schematic drawings of optic discs laser lesions and of series of coronal sections of the dLGN, in three monkeys, depicting the areas of the nucleus deafferented by the lesions.

## KEYWORDS

calbindin, dLGN densitometry, GAP43, GFAP, parvalbumin

## 1 | INTRODUCTION

The use of immunohistochemical methods to study neuronal plasticity enables the correlation of molecular and cellular processes during plastic changes in the adult brain. Calbindin (Cb) and parvalbumin (Pv) are calcium-binding proteins (CaBPs) that are present in various

regions of the central nervous system. They are selectively distributed in many subcortical nuclei and in numerous cortical areas, where they appear to be related to distinct neural pathways and functions (Celio, 1990; Hendry & Jones, 1986; Hof & Nimchinsky, 1992; Jones & Hendry, 1989). In the dorsal lateral geniculate nucleus (dLGN) of primates, Pv is present in relay cells of both the parvocellular (P) and

magnocellular (M) pathways, whereas Cb is mainly detected in the S layers and in the interlaminar zones, which belong to the third visual pathway (Casagrande, 1994; Goodchild & Matin, 1998; Johnson & Casagrande, 1995; Jones & Hendry, 1989; Mize et al., 1992; Soares et al., 2001; Tigges & Tigges, 1991).

Growth-associated protein-43 (GAP43), otherwise known as B-50, F1, pp46, or p57, is related to the initial establishment, regeneration, and functional modulation of synaptic relationships in the central nervous system (Neve et al., 1988). GAP43 is present in large quantities in the developmental stage of the nervous system, where it plays an essential role in axonal growth and synaptogenesis. The biochemical characteristics of GAP43 suggest that some “growth-associated” proteins may alter the neuronal response to extracellular signals by altering intracellular signal transduction systems (Skene, 1989). Experimental lesions in the mammalian CNS revealed a close correlation between regeneration and high levels of GAP43 expression. In mature brains, the expression of GAP43 is less clear but it remains present in the high integration areas of the brain, such as the associative neocortex and the hippocampus. Evidence obtained after a specific immunohistochemical reaction has enabled us to propose that new local synapses are being organized (Baekelandt et al., 1994; Higo et al., 2000; Neve et al., 1988). The expression of GAP43 appears in all layers of the normal LGN, including the interlaminar regions where the koniocellular neurons are located (Higo et al., 2000). After retinal lesions are induced in cats, immunostaining for GAP43 also appears in all layers of the LGN but is more distinct in parvocellular layers (Baekelandt et al., 1994). On the other hand, after monocular deprivation in newborn monkeys, immunostaining for GAP43 is lower in layers 2, 3, and 5 of the dLGN ipsilateral to the deprived eye and in layers 1, 4, and 6 of the contralateral eye (Higo et al., 2000). In macular lesions caused by argon laser irradiation, greater immunostaining appeared in the central area than in the peripheral area of the NGL, and maximum expression was observed in cats 3 weeks after the lesions. The expression of GAP43 in the fifth week was much less clear, although it was detected for up to 7 weeks after injury (Baekelandt et al., 1994).

Glial fibrillary acid protein (GFAP) is a filamentous protein that is expressed in astroglia in mammalian brains. The immunoreaction for GFAP allows researchers to locate and estimate the lesion dimensions in the dLGN according to its retinotopic map (Malpeli & Baker, 1975). Increased immunostaining for GFAP is already observed in the LGN 1 week after retinal lesions, becoming very clear after 3 weeks and persisting up to 7 weeks after injury (Baekelandt et al., 1994; Leal et al., 1997).

We studied the expression of GAP43, GFAP, Cb, and Pv in adult capuchin monkeys after laser-induced lesions were generated at the margin of the optic disc (OD) to study the effects of visual deprivation on the time course of changes in the dLGN. These lesions simulated lesions resulting in glaucoma that have a conspicuous involvement of ganglion cell axons. Unlike previous studies, we generated larger retinal lesions with a laser to study the time course of plasticity in the expression of these proteins in the dLGN. Using a neodymium:YAG laser (Nd:YAG laser) with wavelengths equivalent to an argon laser to generate retinal lesions in ganglion cell axons on the border of the optic

nerve of the capuchin monkey and obeying the spatial-temporal death of these axons, this study has the objective to describe and compare the morphological changes that occur in different processing regions in the visual system (dLGN and V1). In addition, we desired to establish a comparison between the degeneration observed in the dLGN and V1 in the experimental model of lesions in the capuchin monkey with the degeneration of these same structures in the of experimental glaucoma model in monkeys in which the destruction of the trabecula was induced by a laser, as described by Harwerth et al. (1999).

## 2 | METHODS

Four adult male *Sapajus apella* (formerly *Cebus apella*) monkeys weighing between 3 and 4 kg were used in this study. Two of these animals were used in a previous study addressing the cortical plasticity (14). The procedures and protocols followed the NIH guidelines for the Use of Laboratory Animals. The IBCCF/UFRJ research committee approved these procedures (CAUAP-IBCCF/UFRJ, protocol #60-03-2007). Using a hand-held ophthalmoscope, we examined the fundi of the eyes to ensure that the retinas of the animals did not already contain a lesion.

### 2.1 | Paradigm

Plastic changes in the dLGN after acute retinal lesions were evaluated by assessing the time course of the expression of GAP43, GFAP, Cb, and Pv at different time points after injury. The lesions in different portions of the optic disk border were generated with a frequency-doubled neodymium:YAG laser at different time points before animals were euthanized. The retinal lesions were generated with laser shots of different intensity and at different survival time in each animal. We used cytochrome oxidase histochemistry of layer IVc of V1 to determine the topographic location and extent of the lesions based on the appearance of ocular dominance columns (ODCs). This information was used to locate the corresponding site of the dLGN lesion. Protein expression was assessed in coronal sections of the dLGN by determining the relative density of staining of the inferred injured regions compared to that of controls.

### 2.2 | Retinal lesions

Before each session of retinal lesion induction, the animals were anesthetized with 1.5 mL of a mixture of four parts of ketamine (6% Ketalar, Parke-Davis) to one part of xylazine hydrochloride (2% Rompun, Bayer). A mixture of 0.6 mL of atropine sulfate (Atropina, Hypofarma, 0.15 mg/kg) and 0.4 mL of diazepam (Valium, Roche, 0.8 mg/kg) was injected to prevent tracheobronchial secretion and stress. Two drops of ophthalmic solutions of 10% phenylephrine hydrochloride (10% Phenilefrin, Oculum) and tropicamide (1% Mydracyl, Alcon) were applied to the animals' eyes to dilate the pupil and facilitate visualization of the

fundus of the eye. Local anesthetic (100 mg of tetracaine hydrochloride, Allergan-Frumtost) was applied to the cornea. Then, a lens OMRA - WF Mainster Wide Field (Ocular Instruments, Inc., Bellevue, WA, USA) with an objective of 5× soaked in a solution of 2% methylcellulose was positioned on the cornea of the animal. This lens facilitated the visualization of the posterior pole and equator and the retinal periphery (Medeiros, 1997). Lesions at the border of the optic disk were generated at different time points relative to the time of euthanasia. These lesions were induced by photocoagulation with a neodymium laser (OPHTHALAS 532 nm) mounted to a slit ophthalmoscope (TopCon AIT-20 with a Carl Zeiss 30 SL-M, Oakland, NJ, USA). The infrared radiation emitted by the laser crosses the eye without being absorbed by the cornea or crystalline. The wavelength of this laser (532 nm) is well absorbed by melanin and hemoglobin but has little absorption by macular xanthophyll (Barsante & Diniz, 1997; Bozinis, 1997). We used laser shots with pulses of 0.8–0.3 mW and a duration of 200 ms. Animals OD1 and OD2 received pulses of 0.8 mW for 200 ms, while animal OD3 received pulses of 0.3 mW with a duration of 200 ms.

High-power laser shots (0.8 mW) destroy all retinal layers and sever fibers passing through the inner layers of the retina, while low-power laser (0.3 mW) shots disrupt the retinal structure by destroying the outer retinal layers. Lesions to the OD produce a devastating effect on fibers in this passage, resulting in a larger scotoma than similar lesions in other portions of the retina. Similar shots administered to the retina destroy photoreceptors and exert a much smaller effect on fibers in this passage (14). The degree of plasticity in the cortex depends on the location and amount of energy of the laser shots. We used contiguous laser shots (8–16) at the border of the optic disk. The number of shots varied according to the extent of the lesion. Most lesions were made by 8–12 shots. In Case OD1, we used high-power laser shots, similar to those used previously (Farias et al., 2019), but the lesions were large and showed a high degree of edema. In Case OD3, the intensity of the laser shots was reduced by 35%.

We used a paradigm of massive lesions of ganglion cell axons with laser shots administered to the margin of the OD. Massive laser-induced retinal lesions destroy most retinal fibers at the border of the OD. This paradigm, which is illustrated in Figure 1, is based on the administration of multiple high-power laser shots at the border of the OD at different time points before euthanasia in Cases OD1, OD2, and OD3. The resulting ODCs appear on the flattened representations in V1 (Figure 3d) and on sections of dLGN in the areas corresponding to the retinal lesions (Figure 1a–c). The lesions were generated starting from the periphery of the retina (older lesions) and ending at more central regions (more recent lesions). This procedure avoided destroying fibers in the passage that might mask deafferentation of control regions of the retina. The original paradigm, which is based on the data obtained from macaques, was designed to compare the staining density of GAP43, GFAP, Pv, and Cb in the dLGN layers ipsilateral to the lesion in the OD. The layers of the dLGN in macaques are illustrated in a parasagittal section (Figure 1d) and in a series of coronal sections (Figure 1e). The series stained using the Nissl method were used to delimit the layers. Thus, the initial paradigm involved comparing the deafferented layers (ipsilateral) with the uninjured lay-

ers in the same histological section of the dLGN (Figure 1f). However, the dLGN in capuchin monkeys does not show a clear segregation of the layers throughout the nucleus (7). Therefore, the original paradigm was modified to analyze the staining density of all parvocellular layers combined, the magnocellular layers combined, and the S layer at each postinjury time point (Figure 1g). Figure 2(b) shows a coronal section of the dLGN from a capuchin monkey, with anatomical subdivisions. The sections of the dLGN containing the S layer were divided into three parts: magnocellular, parvocellular, and S layers. Parvocellular layers of the dLGN in capuchins are not clearly segregated. Nonetheless, we added white dashed lines at the borders of the parvo, magnocellular, and S layers in the Nissl-stained coronal section (Figure 2b). This segregation is often not visible in sections stained for immunohistochemistry. For this reason, the densitometry analysis was made in lesions and nonlesioned areas in all layers combined. After all lesions were generated, fundus photographs were captured with a fundus camera (TopCon TRC - 50 WENT Retinal Camera, Tokyo, Japan) coupled to a charge-coupled device (CCD) video camera. Figure 2(a) shows a fundus photograph of the left eye of Case OD2 after the last lesion. It shows the result of laser lesions at the border of the OD. The limits between the lesions induced at 52 and 2 days are indicated by asterisks, and the nonaffected nasal border is between the white lines. The lesions of all retinas were photographed with a fundus camera. Only retinas from cases OD1 and OD2 were dissected and the retinas were included in paraffin, stained with hematoxylin and eosin. Photomicrograph of the retina was included in a previous study (Farias et al., 2019).

We used the massive lesion paradigm in Cases OD1, OD2, and OD3. These lesions were generated with laser shots (0.3–0.8 mV, 0.2 s) at the border of the right OD at different time points before euthanasia: 25, 3, and 1 day in case OD1; 52 and 2 days in case OD2; and 30, 9, and 3 days in case OD3. The lesions destroyed fibers in the passage derived from large portions of the retina. Figure 3 shows schematic diagrams of the cortical results of the massive lesion paradigm used in Cases OD1, OD2, and OD3. The areas of the right retina with ganglion cell degeneration involved almost the entire visual field representation, sparing only the central lower field representation. These lesions resulted in deafferented regions of the left (LH) and right (RH) hemispheres, as evidenced by the appearance of ODCs at the cortical representation of V1 observed at the flattened preparations of layer IV (Figure 3d). In one case (OD4), no lesions were made, and this case served as a control (Figure 6d, 6h, and 6k).

### 2.3 | Flattened maps and assessment of the extent of the lesions

After different survival periods, the animals received lethal doses of sodium pentobarbital (100 mg/kg, IV) and were perfused through the heart with 0.9% saline followed by 2% paraformaldehyde in 0.1 M phosphate buffer saline (PBS). The eyes of the animals were removed, cut at the equator, and photographed with the aid of a CCD camera mounted on a Nikon stereomicroscope.

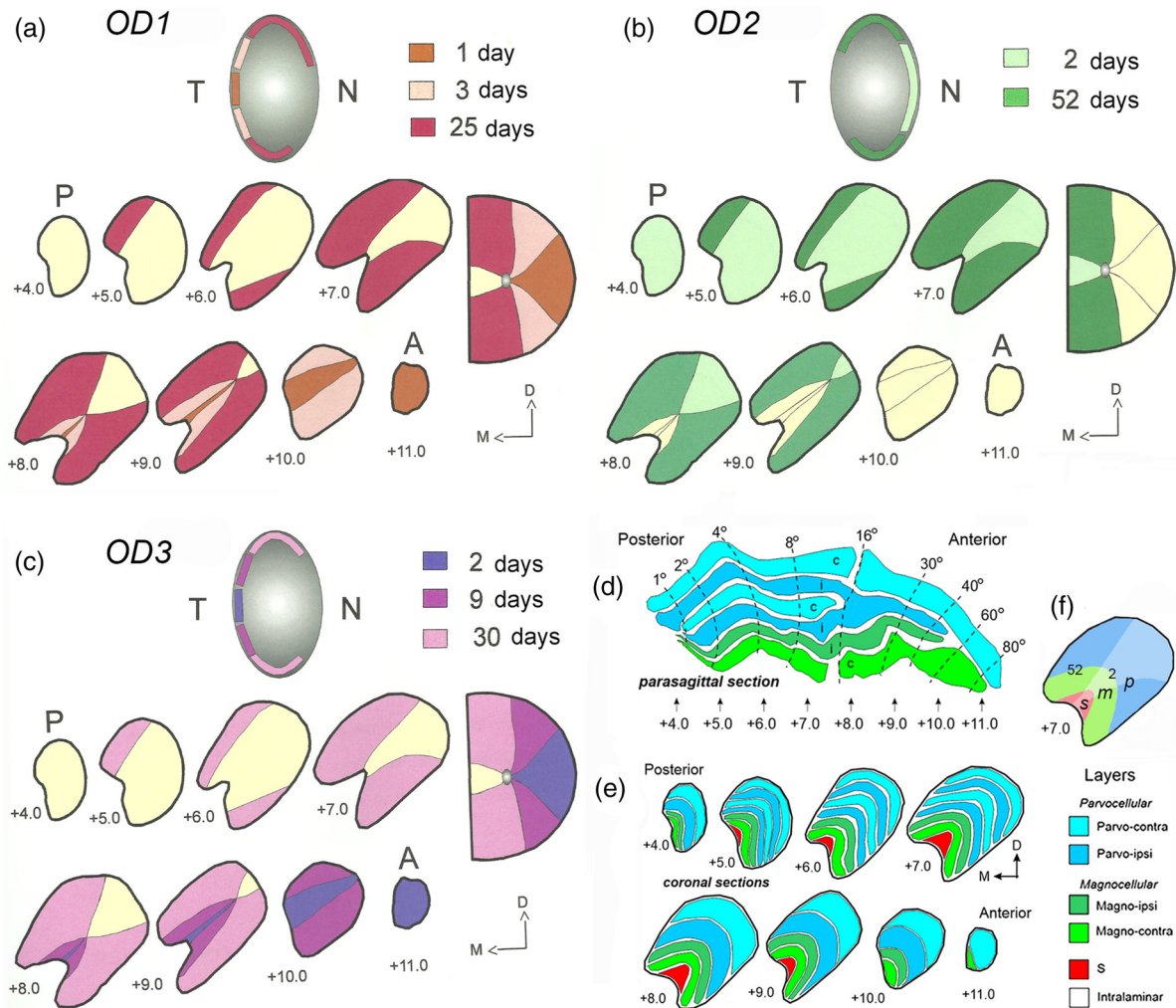


**FIGURE 1** Schematic drawings of optic discs with the laser lesions and of series of coronal sections of the dLGN of three monkeys depicting the areas of the dLGN deafferented by the lesions. (a) Schematic diagrams of the massive lesion paradigm used in Case OD1. Top: Lesions made at the border of the right optic disc at different times. Lower right: Series of coronal sections of the dLGN showing the deafferented areas in different colors representing lesions at the optic disc in the different times. (b) and (c) are schematic diagrams of the massive lesion paradigm used in Cases OD2 and OD3. (d) Parasagittal section of dLGN in the macaque showing the contralateral (light blue) and ipsilateral (medium blue) parvocellular layers and the ipsilateral (medium green) and contralateral (light green) magnocellular layers. (e) Coronal sections throughout the dLGN with the expected parvocellular, magnocellular, and S layers (red) in capuchin monkeys. (f) Protocol used in capuchins due to the uncertainty of the borders of the layers (for details, see text). Scale bar = 750  $\mu$ m

The brain was removed from the skull, and the posterior portion underwent the flat-mounting procedure to obtain flat preparations of V1 (Farias et al., 2019). Flat-mounted blocks were fixed between parafilm-covered glass slides with a solution of 4% paraformaldehyde in 0.1 M PBS for 6 h, followed by 4% paraformaldehyde + 2.5% glycerol for 3 h and 4% paraformaldehyde + 5% glycerol for 3 h. Then, the blocks were incubated overnight in PBS/30% sucrose. Afterward, the blocks were quickly frozen and cut at a thickness of 40  $\mu$ m using a freezing microtome. The CytOx histochemical reaction was performed using the protocol described by Wong-Riley (1979), as modified by Silverman and Tootell (1987, Method II). Sections stained for CytOx were photographed under blue light illumination using high contrast film (12 ASA, Kodalith™, Kodak Co.).

The use of CytOx histochemistry allows the direct visualization of OD stripes in layer IV of V1 and indirect visualization of the limits of the representative area of the retinal lesion (Farias et al., 2019). Figure 3(a)–(b) (Rosa et al., 1988) shows the extent of the lesion, as revealed by the ODCs in V1 and translated to visuotopic coordinates using the method proposed by Gattass et al. (1987) for V1. These coordinates were transferred to the dLGN using the visuotopic map proposed by Malpeli and Baker (1975) for the macaque dLGN. The stained sections of V1 were photographed with high-contrast film using Leitz Aristophot. The negatives were enlarged 7X and copied onto standard Kodabromide photographic paper. We prepared manual photographic reconstructions of ODCs in all animals. Manual reconstruction was performed starting from the cutting, assembly,

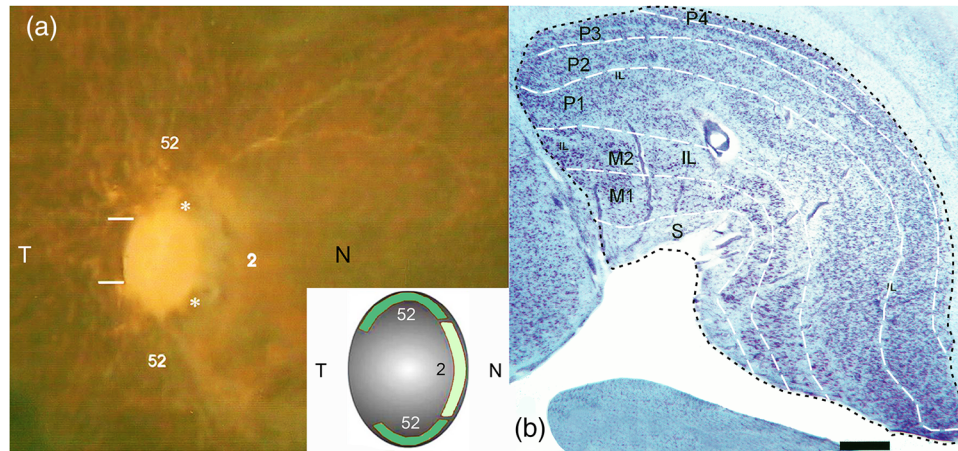


**FIGURE 2** Photograph of the fundus of the eye and of a coronal section of the dLGN. (a) Posterior pole of the right eye presenting the results of laser lesions at the border of the optic disc in Case OD2. Nonlesioned temporal border of the optic disk is between white horizontal lines, while the limits between the lesions made at 52 and 2 days are indicated by asterisks. The early lesions (52 days prior to the euthanasia) are delimited by white horizontal bar an asterisk dorsal and ventrally, while the late lesion, 2 days prior to the animal sacrifice are delimited by asterisks. (b) Photomicrograph of a coronal section of the dLGN of a normal capuchin monkey. Four parvocellular layers (P1–P4), two magnocellular layers (M1–M2), one S layer (S), and at least three interlaminar layers (IL) are shown at this level. Scale bar = 750  $\mu$ m. For details, see text. ((a) is another photograph of the optic disc shown in figure 5 of Farias et al., 2019)

and collage of photos of several sheets. Ultimately, two reconstructions of layer IVc of V1 were generated for each case, one for each hemisphere.

## 2.4 | Histological processing

The retinas of Cases OD1 and OD2 were dissected from the eye and photographed with an Olympus camera to visualize the effects of the laser shots. The eye cups with the retina were dehydrated and embedded in liquid paraffin at a medium temperature of 56°C. The paraffin-embedded tissue was cut to a thickness of 15  $\mu$ m. The sections were mounted on glass slides, defatted, and stained with hematoxylin and eosin.

The remaining portion of the brain containing dLGN was incubated with 2% paraformaldehyde in PBS + 2.5% glycerol for 6 h, followed by PBS + 5% glycerol for 12 h and PBS + 10% glycerol overnight. Serial 40- $\mu$ m-thick coronal sections were obtained using a cryostat. Adjacent series were stained with cresyl violet to label the cell bodies, with Gallyas' method to label myelin (Gallyas, 1979), and with immunocytochemistry using antibodies against GAP43, GFAP, Cb, and Pv.

For immunocytochemical reactions, free-floating sections were incubated overnight with anticalbindin D-28k (1:2500), mouse monoclonal 300 IgG1 (Swant, Bellinzona, Switzerland), antiparvalbumin 235 (1:3000), mouse monoclonal IgG1 (Swant, Bellinzona, Switzerland), anti-GAP43 (1:2000) mouse monoclonal IgG1, sc-17790 (Santa Cruz Biotech., CA, USA), or anti-GFAP (1:2000) rabbit polyclonal 7696 (Swant-Swiss Antibodies, Bellinzona, Switzerland) antibodies in a solution containing 0.05% bovine albumin and 0.3% Triton X-100 in 0.001 M PBS, pH 7.4. The sections were rinsed three times

with PBS and then incubated for an additional hour with a biotinylated antimouse (for Cb and Pv) or antirabbit (for GFAP and GAP43) secondary antibody (1:200) in PBS containing 5% normal horse or goat serum at room temperature. Sections were rinsed again with PBS and then processed using the avidin–biotin method with ABC kits (Vector Laboratories, Burlingame, CA, USA) for 1 h and 0.05% 3,3'-diaminobenzidine (DAB; Sigma-Aldrich Inc, Ca, USA) in PBS containing 0.001% H<sub>2</sub>O<sub>2</sub> for 5 min. The sections were rinsed with PBS and mounted onto gelatinized glass slides, dehydrated through graded alcohol solutions, air-dried, and coverslipped with DPX. No labeling was observed in control sections where primary antibodies were omitted.

## 2.5 | Densitometry

Stained sections were examined with a fluorescence microscope (Leitz Orthoplan 2, Leitz) and photographed with a digital camera (Leica-wild MPS48, Leitz). Lamina borders in the lateral geniculate nucleus were determined by comparing immunostained sections with adjacent sections stained with cresyl violet. The images were ordered such that each assembly contained the corresponding section of Nissl, GAP43, GFAP, Cb, and Pv staining for the dLGN ipsilateral and contralateral to the lesioned eye. For each reaction or staining, nine sections representing dLGN areas corresponding to different eccentricities in the visual field, as shown in Figure 1, were selected. Selected images of the dLGN in coronal sections were also divided into two or three parts, corresponding to the magnocellular, parvocellular, and S layers. Each of these parts was divided into other parts (Figure 1f) that correspond to the dLGN projection of the damaged area on the optical disc, according to its temporal variation, and visual topography based on the divisions

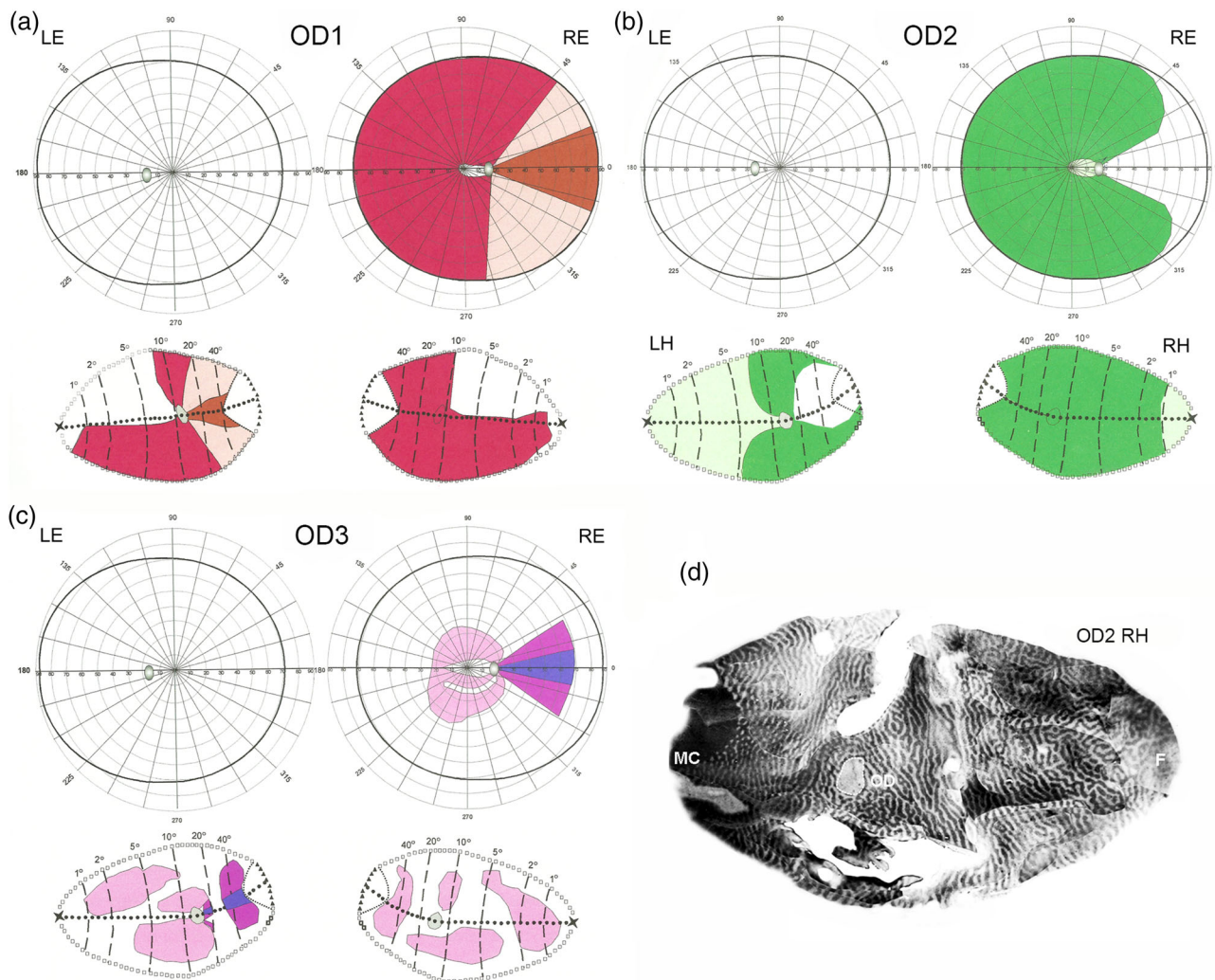


**FIGURE 3** Schematic reconstructions of lesion zones in the visual field and in the layer IVc of V1 of the right (RH) and left hemispheres (LH) in Cases OD1 (a), OD2 (b), and OD3 (c). (d) Photomicrograph reconstruction of the flattened map of layer IVc of the case OD2. The deafferented regions of the schematic diagram can be correlated with the pattern of ocular dominance columns (ODCs) in layer IVc. Compare the green regions of the left hemisphere in Case OD2 with the location of the ODC in (d). We used different color brightness to delineate the deprived areas for each time prior to the euthanasia. The lesions in each animal were presented with different colors. (F, fovea; OD, optic disc; MC, monocular crescent). Two of these animals were used in previous study the neural plasticity of the striate cortex (Farias et al., 2019)

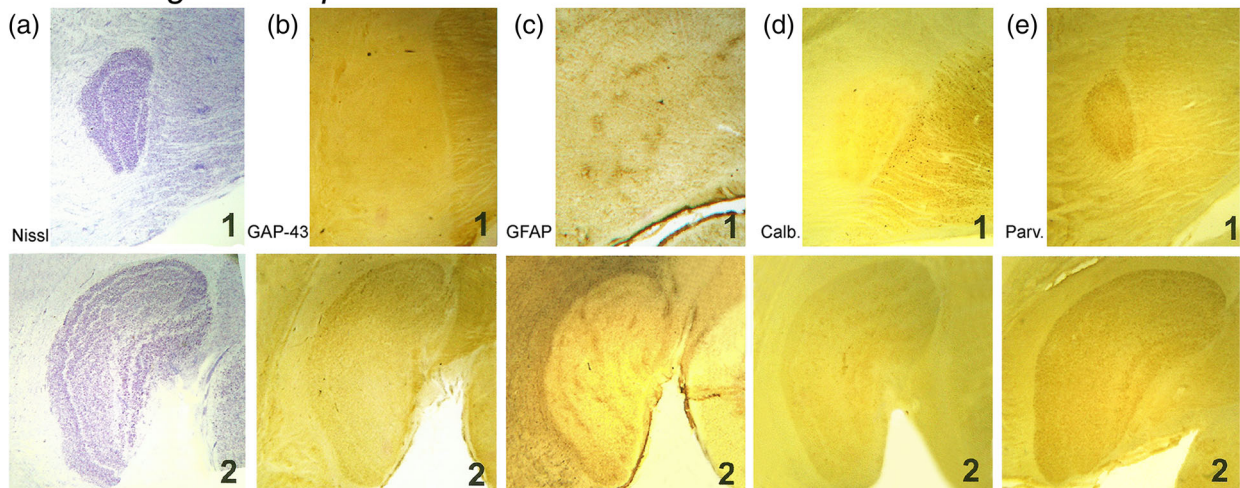
described by Malpeli and Baker (1975). The color information was removed from the sections using Adobe Photoshop 5.5 software (Adobe Co., San Jose, California, USA). Densitometry of black and white images of portions of the dLGN was accomplished with the aid of the Image Analyzer program (ImageJ 1.46r courtesy of NIH, Bethesda, MD (downloaded from <http://imagej.nih.gov/ij>).

The regions corresponding to the different postlesion time of the Parvo, Magno, and S layers were further subdivided for the analysis of the image program. We produced equal number of fragments for each postlesion time for each layer. The resulting image of the fragments was subjected to the densitometry analysis. The image program would systematically label each fragment and supply the mean density stain and their standard deviation for each fragment.

For illustration purpose, three sections representing dLGN areas corresponding to two or three eccentricities in the visual field were

selected: 5° centers, between 5° and 10°, and between 15° and 25°. Because the dLGN of the capuchin has an average size of 6.5 mm, the sections chosen were located at 0.5, 1–1.5, and 3.5 mm beginning the posterior dLGN and corresponding to the coronal Horsley & Clark planes +4.0, +6.0, and +8.0, as identified in Figures 4 and 5(a) by numbers 1–3. When we did not have sections corresponding exactly to these coordinates, we used the coronal plane closest to the planned plane. Portions of the images corresponding to the lesioned eye were grouped according to the reaction to which they were submitted and the time of the lesion and analyzed by their transmittance using a computer running the image analyzer program. The analyzed groups were numbered according to the animal, the studied dLGN (ipsilateral or contralateral), the layer (magnocellular, parvocellular, or S layer), and the survival time after the lesions. Combinations of groups corresponding to monkeys with similar lesions were also established, namely,

## OD3 - right hemisphere



## OD2 - left hemisphere

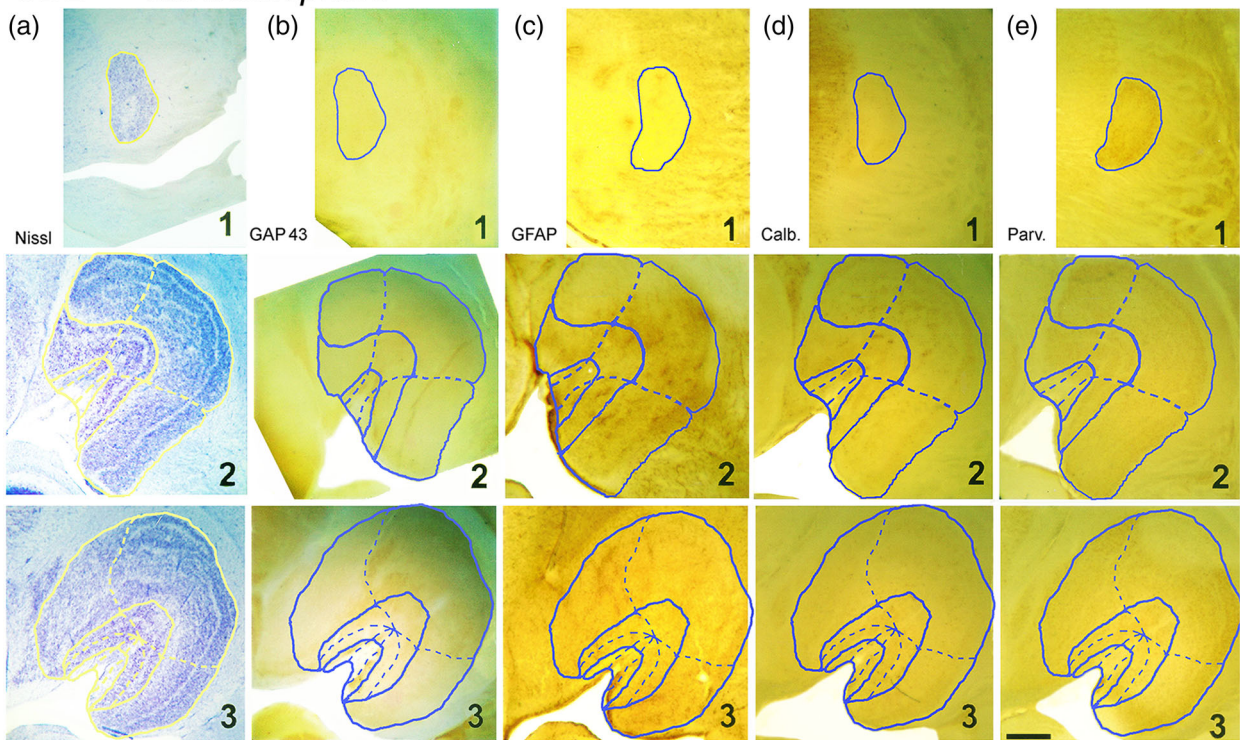


**FIGURE 4** Photomicrograph of coronal sections of the right dLGN in Cases OD3 (top) and OD2 (bottom), stained for Nissl(a), GAP-43 (b), GFAP (c), calbindin (d), and parvalbumin (e) at different anterior posterior levels. The sections are located at the representation of the central visual field (1 = +4.0); and at the representation of 5–10 degrees (2 = +6.0); and at the representation of 10–15 degrees (3 = +8.0 in Horsley–Clark anterior posterior [AP] coordinates). Case OD3 (top) is illustrated with no overlay. In Case OD2 (bottom), the border of the dLGN layers (solid lines) and of the different lesion time (delimited by dashed lines) were overlaid onto the sections. Note in the dorsal portion of the Case OD3, the increased density for the GAP43 in the parvocellular layers of sections 2, and in Case OD2, the increased density for the GAP43 and GFAP in the parvocellular layers of sections 2 and 3 corresponding to the lesion made 2 days prior to euthanasia (middle dorsal portion of the LGN). Scale bar = 750  $\mu$ m

monkeys OD1 and OD3, whose lesions were located nasal to the OD. The numerical optical density data were submitted to nonparametric statistics using SYSTAT 8.0 (Systat Software, Inc., Chicago, Illinois, USA). Analysis of variance (ANOVA) with the post-hoc Tukey test for multiple comparisons was used. Generally, the ipsilateral layers were

not analyzed independently from the contralateral layers due to the difficulty of separating the parvocellular layers in capuchin monkeys.

The densitometry data obtained for each immunoreaction and for each dLGN layer were transformed as the “protein expression index” (PEI). The image analyzer program determines the transmittance,

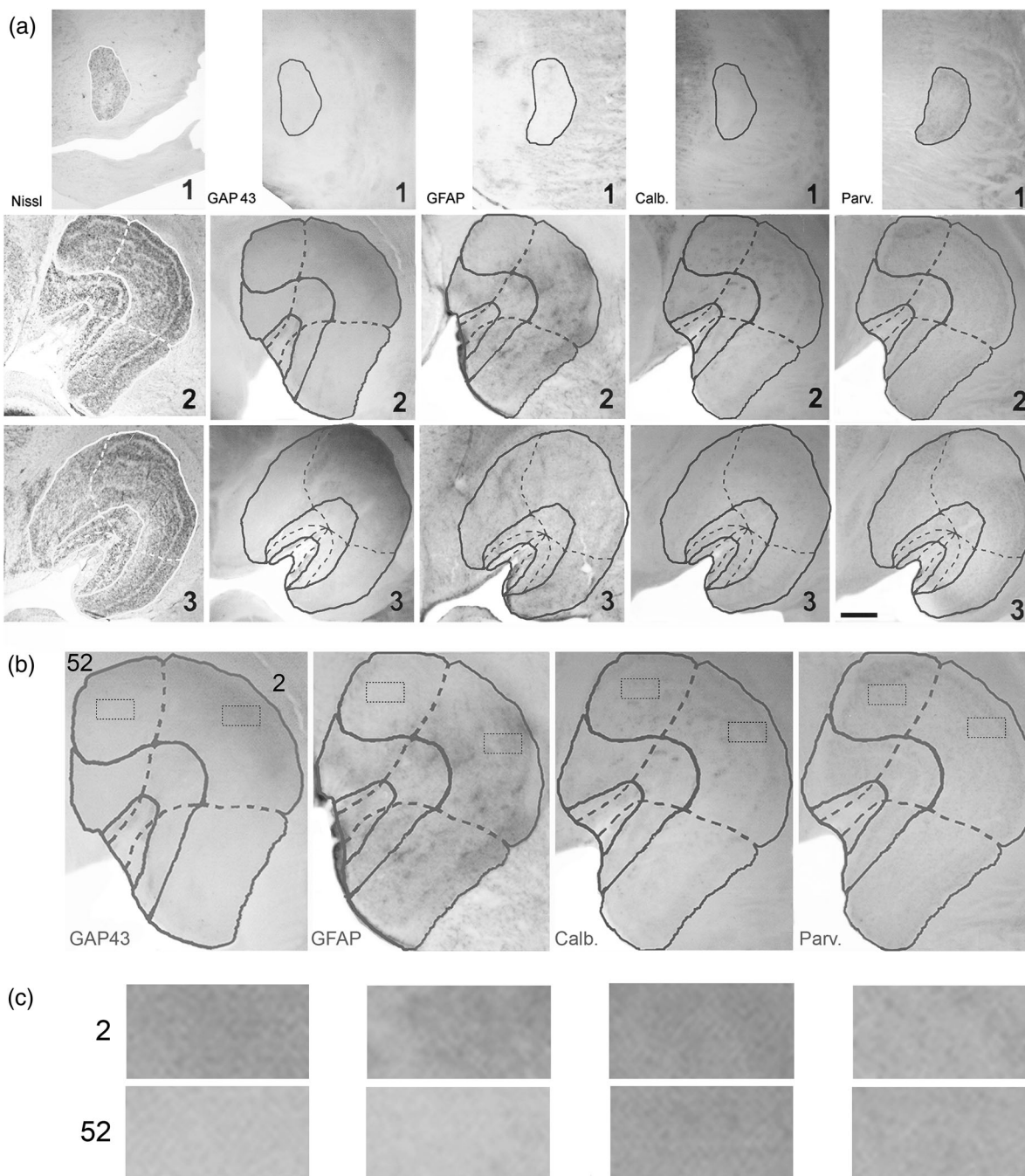


**FIGURE 5** Staining density of parvocellular portions of the dLGN in coronal sections stained for GAP-43, GFAP, calbindin, and parvalbumin of Case OD2. (a) Same sections showed in Figure 4 bottom, in black and white. (b) Sections located at the representation of 5–10 degrees (2 = +6) showing the location of the samples corresponding to 2 and 52 postlesioned areas. (c) Samples of staining density corresponding to the dashed square shown in (b). See also legend for Figure 4. Scale bar in (a) = 750  $\mu$ m

which is inversely proportional to the density; namely, a denser section is less bright. The PEI was calculated by dividing the mean values obtained in the control uninjured regions by the average values corresponding to the lesion days. A PEI > 1 indicates that the analyzed segment has the highest expression of the indicated protein compared with the control regions. A PEI < 1 indicates that the expression of the protein studied is lower than that detected in noninjured segments.

### 3 | RESULTS

Using Nissl-stained sections, we determined the locations of the parvocellular, magnocellular, and S layers in each immunoreacted section. Examples of these sections are shown in Figure 4 (bottom) and Figure 5(a). Figure 4 shows coronal sections of the right dLGN from cases OD3 (contralateral) and OD2 (ipsilateral) stained for Nissl (A),

**TABLE 1** Transmittance of GAP43-stained sections for magno, parvo, and S layers and for each postlesion period in each animal

Layers	Days	Magno		Parvo		S		M-PEI	P-PEI	S-PEI
		Mean	SD	Mean	SD	Mean	SD			
GAP43	C	104.040	8.079	103.040	14.698	93.590	2.178	1.000	1.000	1.000
	1	73.965	28.829	58.000	16.971	77.855	23.879	1.407	1.777	1.202
	OD1	3	95.180	25.119	72.750	10.982	92.035	37.818	1.093	1.416
GAP43	25	108.341	17.740	108.671	24.656	92.955	7.106	0.960	0.948	1.007
	C	74.830	4.665	68.247	4.199	54.133	8.663	1.000	1.000	1.000
	5	75.110	0.000	91.223	15.375	47.010	0.000	0.996	0.748	1.152
OD2	55	62.378	9.676	88.738	17.988	56.270	0.000	1.200	0.769	0.962
GAP43	C	108.895	13.103	119.312	39.740	102.255	6.498	1.000	1.000	1.000
	2	50.115	23.568	63.015	35.843	31.990	12.544	2.173	1.893	3.196
	OD3	9	45.825	12.456	66.468	33.173	38.523	15.222	2.376	1.795
	30	75.861	36.772	101.215	32.249	92.680	0.000	1.435	1.179	1.103

**TABLE 2** Transmittance of GFAP stained sections for magno, parvo, and S layers and for each postlesion period in each animal

Layers	Days	Magno		Parvo		S		M-PEI	P-PEI	S-PEI
		Mean	SD	Mean	SD	Mean	SD			
GFAP	C	111.647	24.593	93.003	39.522	114.600	18.767	1.000	1.000	1.000
	1	66.040	21.128	43.265	29.720	107.380	0.000	1.691	2.150	1.067
	OD1	3	94.140	23.439	50.510	38.623	125.020	0.933	1.186	1.841
GFAP	25	104.635	33.115	99.301	32.496	137.850	28.115	1.067	0.937	0.831
	C	119.470	14.637	85.870	17.550			1.000	1.000	
	2	101.890	16.391	80.960	18.123	132.920	0.000	1.173	1.061	
OD2	52	119.776	17.197	97.920	27.838			0.997	0.877	
GFAP	C	83.015	53.860	99.780	26.225	77.500	52.283	1.000	1.000	1.000
	2	63.345	28.291	57.145	7.715	73.925	33.877	1.311	1.746	1.048
	OD3	9	69.985	30.594	68.472	13.713	99.880	2.913	1.186	1.457
	30	90.040	25.579	98.449	26.782	90.460	0.000	0.922	1.014	0.857

GAP43 (B), GFAP (C), Cb (D), and Pv (E) at different anterior–posterior levels. The mean and standard deviation of the section transmittance were determined for each layer and for each postlesion period for sections stained with antibodies against GAP43 (Table 1), GFAP (Table 2), Cb, and Pv (Table 3). Changes in staining density are barely noticeable in individual colored coronal sections. Subtle changes are visible in sections stained for GAP43 in the dorsal portion of the dLGN in Case OD3 (Figure 4, top), corresponding to the lesion area (see Figure 3c) and in the middle portion of the dLGN in Case 2 (Figure 4 bottom) in sections stained for GAP43 and GFAP. In Figure 5(a), where the color information was removed, we saw differences in density among the portions with different time after the lesion. See, for instance, the density of staining in the center versus the lateral and medial portions of the dLGN in sections stained for GAP43. Figure 5(b) shows enlarged version of the sections of GAP43, GFAP, Cb, and Pv of one anterior–posterior levels shown in Figure 5(a). Examples of portions of the sections corresponding to nonlesioned and lesions areas are

shown in Figure 5(c). The samples of the dLGN corresponding to the lesioned portions representing 2 and 52 postlesion time show different stain density. Data analysis was made systematically using the results of the mean density stain of the black and white fragments of each reaction. The results for each layer are well documented in the bar graphs (Figures 6 and 7) and in Tables 1–3.

### 3.1 | GAP43

In Case OD1, protein expression was increased in the magnocellular layers at only 1 day after the lesion was induced in the nasal sector. On day 3, GAP43 levels decreased. On the 25th day after the lesion was established in the upper and lower sectors, GAP43 levels had already returned to normal (Figure 6a). Similarly, we observed an increase and decrease in GAP43 levels in the parvocellular layers at the same time, but with a higher intensity than in the magnocellular layers (Figure 6b).

**TABLE 3** Transmittance of calbindin- and parvalbumin-stained sections for magno, parvo, and S layers and for each postlesion period in animals OD1 and OD3

Layers	Days	Magno		Parvo		S		M-PEI	P-PEI	S-PEI
		Mean	SD	Mean	SD	Mean	SD			
Calbindin	C			107.392	32.529	55.720	0.000		1.000	1.000
	2	81.947	13.689	76.605	1.011	62.115	0.304		1.402	0.897
	OD3	9	78.385	7.599	79.018	11.551	70.335	3.333		1.359
Parvalbumin	30	82.803	15.259	103.700	20.118				1.036	
	C	104.770	2.489	106.970	9.285			1.000	1.000	
	1	85.700	0.000	55.590	0.000	52.810	0.000	1.223	1.924	
Parvalbumin	OD1	3	78.260	18.116	61.545	2.341	60.000	15.669	1.339	1.738
	29	106.230	17.638	115.557	15.445			0.986	0.926	
	C	103.770	9.164	114.384	6.978	102.310	0.000	1.000	1.000	1.000
Parvalbumin	2	71.905	9.185	71.860	9.221	57.580	8.598	1.443	1.592	1.777
	OD3	9	75.453	11.653	72.248	7.837	67.490	10.488	1.375	1.583
	30	91.071	25.494	113.168	20.382	78.970		1.139	1.011	1.296

In the S layer, a slight increase in GAP43 expression was observed, which returned to normal levels on the 25th day (Figure 6c). ANOVA of the data corresponding to the magnocellular, parvocellular, and S layers showed significance only in the parvocellular layer ( $p = .021$ ).

In Case OD2, the lesions were located in the upper, lower, and temporal sectors. The intensity of the laser shots was lower than in Case OD1, and the number of tissue samples was insufficient for a reliable analysis of GAP43 expression (Table 1).

In Case OD3, the lesions were topographically similar to those of animal OD1, but they were generated with a lower laser intensity than in the first case. The increase in GAP43 expression in the magnocellular layers lasted longer than that in OD1, decreased on the 30th day, and did not reach normal values (Figure 6a). In the parvocellular layers, GAP43 expression increased on the second day, remained stable until the ninth day, and decreased on the 30th day without reaching normal values (Figure 6b). In layer S, an increase in GAP43 expression was noted on the second day after injury in the nasal sector. Nine days after the establishment of upper and lower nasal lesions, GAP43 expression remained high and returned to levels closer to normal 30 days after the generation of upper and lower lesions (Figure 6c). The expression of GAP43 was similar in all layers (Figure 6d) in the control case (OD4), but it was lower than the expression observed in the lesioned cases.

For statistical analyses, we combined the data from animals OD1 and OD3 (Figure 7). This figure shows a similar pattern for the magnocellular and parvocellular layers to that observed for animal OD1, whereas the data for layer S from these two cases were similar to those of Case OD3 (see Figures 6 and 7). ANOVA of the dataset of Cases OD1 and OD3 showed that the variation in GAP43 expression in the magnocellular layers was not significant ( $p = .062$ ), whereas it was highly significant in the parvocellular layers ( $p = .001$ ). Finally, no significant differences were observed in the S layer of the combined sample of Cases OD1 and OD3. Notably, no variation in GAP43 expres-

sion was observed in any of the three layers of the uninjured monkey OD4 (Figure 7d).

### 3.2 | GFAP

An analysis of Case OD1 shows that the magnocellular and parvocellular layers displayed the same pattern of GFAP expression as observed for GAP43 (see Figure 6d and e). Layer S showed a slight increase in GFAP expression 1 day after the nasal lesion was established and decreased to levels lower than normal after 3 days. This level remained below the normal levels 25 days after lesions were generated in the upper and lower quadrants (Figure 6f).

In Case OD2, the expression of GFAP in the magnocellular layers increased 2 days after temporal injury of the optic disk border. After 52 days, the expression of GFAP returned to normal levels. In the parvocellular layers, GFAP expression increased slightly after 2 days. After 52 days, its levels are slightly below normal. In the S layer, no lesion was detected, and the levels of GFAP expression remained normal (Table 2).

In Case OD3, the pattern of GFAP expression differed from that of GAP43 in the magnocellular layers. In this case, GFAP levels were increased at 2 days after injury but decreased after 9 days and were slightly below normal after 30 days (Figure 6d). In the parvocellular layers (Figure 5e), the pattern was similar to that of GAP43, with an increase in expression on the second day and a progressive decrease until reaching normal values after 30 days. In the S layer (Figure 6f), GFAP expression resembled GAP43 expression, as these proteins were expressed at normal levels on the second day, decreased on the ninth day, and increased slightly (but still below normal levels) on the 30th day.

When we assessed the combined data from animals OD1 and OD3, we noticed that GFAP expression in the magnocellular and parvocellular layers increased in the first days after injury, returning to levels

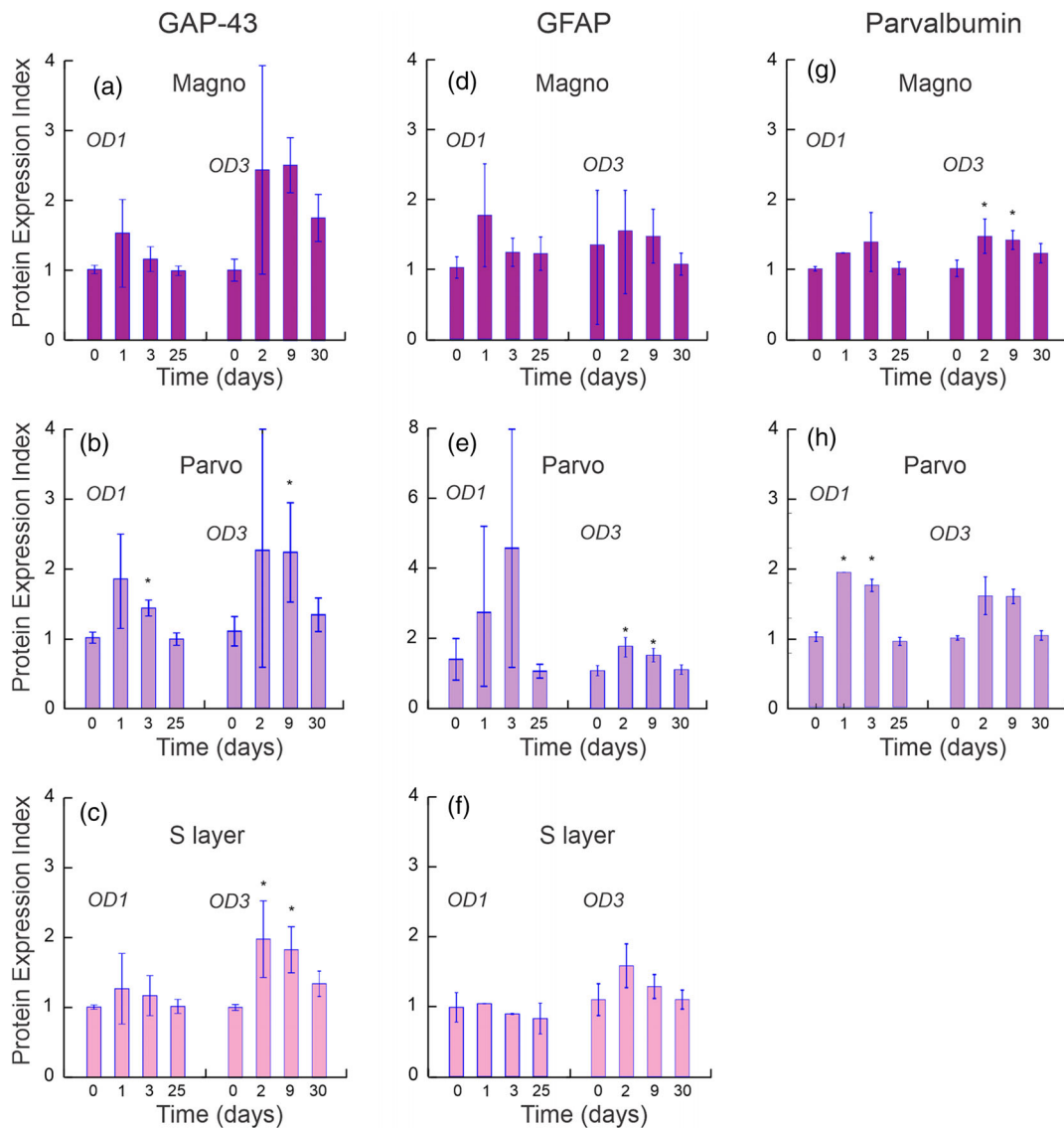


**FIGURE 6** Variation of protein expression index as a function of the postlesion time in Cases OD1 and OD3. The graphs show the mean and standard deviation of transmittance for each region corresponding to the different lesion times for GAP43 (left), GFAP (middle), and parvalbumin (right). Error bars, S.E.M.

slightly below normal after 25 days (Figure 7e and 7f). No significant differences were observed in the magnocellular ( $p = .185$ ) and S ( $p = .462$ ) layers of the combined sample of cases OD1 and OD3. However, the difference was significant for the parvocellular layers in these cases ( $p = .002$ ). The expression of GFAP was similar in all layers in the control case (OD4), but was lower than that in the lesioned cases. In this case, no change in GFAP expression was detected (Figure 7h), similar GAP43 expression (Figure 7d). Therefore, the expression of GFAP was similar in all layers (Figure 7h).

### 3.3 | Parvalbumin

When we examined the histograms of Pv expression in the magnocellular layers in Case OD1, we noticed that its variation was smaller than

that of GAP43 and GFAP. The expression of PV increased at 3 days after injury and returned to the normal level at day 25 (Figure 6g). For the parvocellular layers, the pattern was similar to that observed for GAP43 and GFAP (Figure 6h). Data from layer S were not sufficient for a reliable analysis (Table 3), and the histogram is not illustrated.

In Case OD3, the pattern of PV expression in the magnocellular layers increased on the second day and decreased until the 30th day, although above normal values were maintained (Figure 6g). In the parvocellular layers, PV expression remained at high levels from the second to the ninth day after injury and returned to normal levels on the 30th day (Figure 6h). In the S layer, PV expression was not detected in a sufficient number of sections from Case OD1, and thus, the histogram is not shown (Table 3).

The combined analysis of data from animals OD1 and OD3 showed increased PV expression in the magnocellular layers at 1 day after

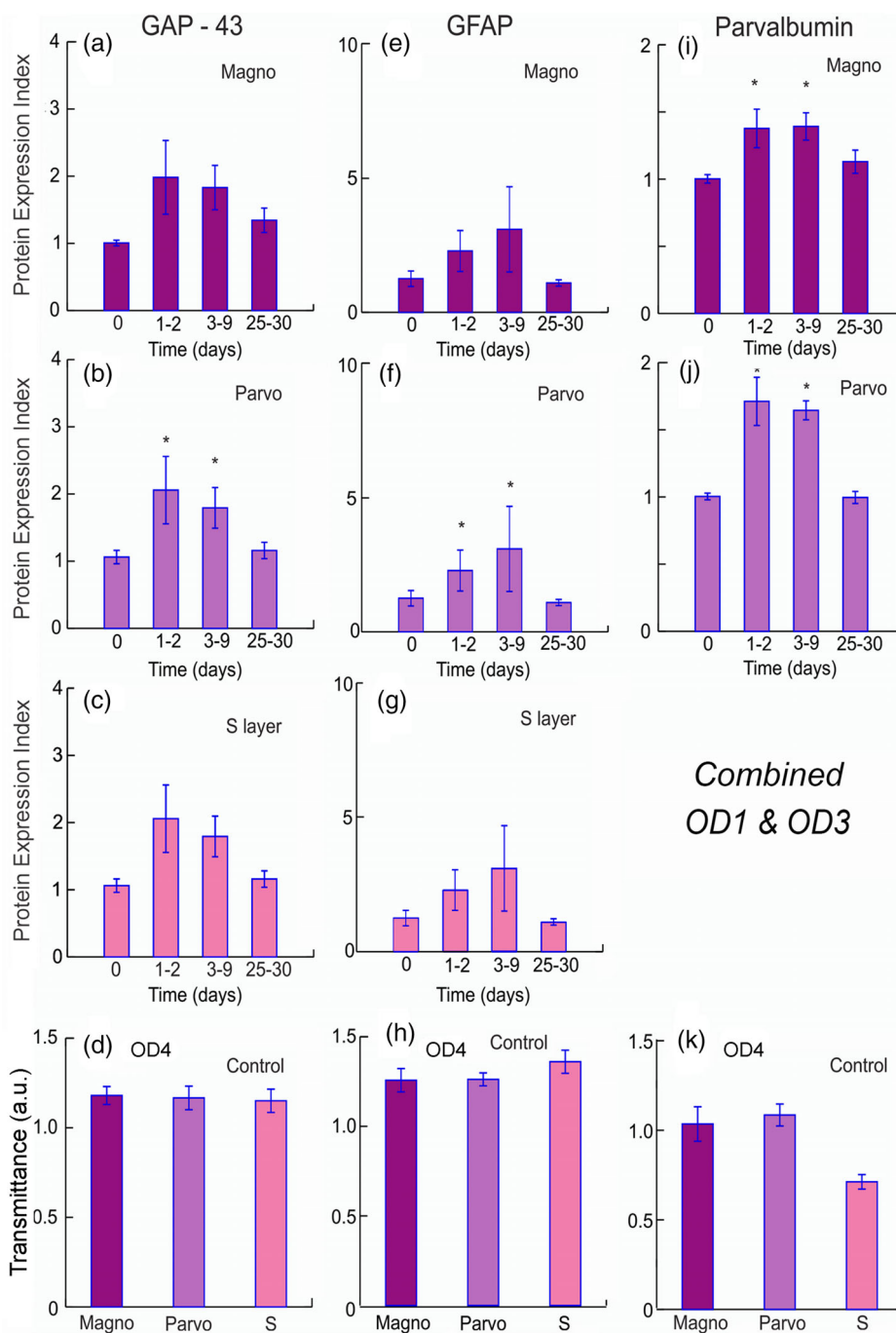


**FIGURE 7** Variation of protein expression index as a function of the postlesion time in Cases OD1 and OD3 (combined) and of transmittance in Case OD4 (control). The graphs show the mean and standard deviation of protein expression index of GAP43 (left, a–c), GFAP (middle, e–g), and parvalbumin (right, i–j) for each region of the dLGN corresponding to the different lesion times for Cases OD1 and OD3 combined. The transmittance (in arbitrary units, a.u.) for each layer and for each stain (d, h, and k) is shown for Case OD4. Error bars, S.E.M.

injury, the expression remained at this level for up to 9 days and returned to near normal levels after 25 days (Figure 7i). The parvocellular layers showed a pattern similar to that of the magnocellular layers (Figure 7j). We do not present a histogram for the S layer (Table 3). ANOVA of the combined data for Pv expression in Cases OD1 and OD3 showed significant differences in the magnocellular ( $p = .046$ ) and parvocellular ( $p = .000$ ) layers.

### 3.4 | Calbindin-D 28k

Only sections of the dLGN from Case OD3 showed a successful reaction for calbindin-D (Cb). The expression of Cb in the magnocellular layers increased on the second day after lesioning and decreased slightly until the 30th day, remaining at above normal levels (Table 3). In the parvocellular layers (Table 3), the pattern was more similar to

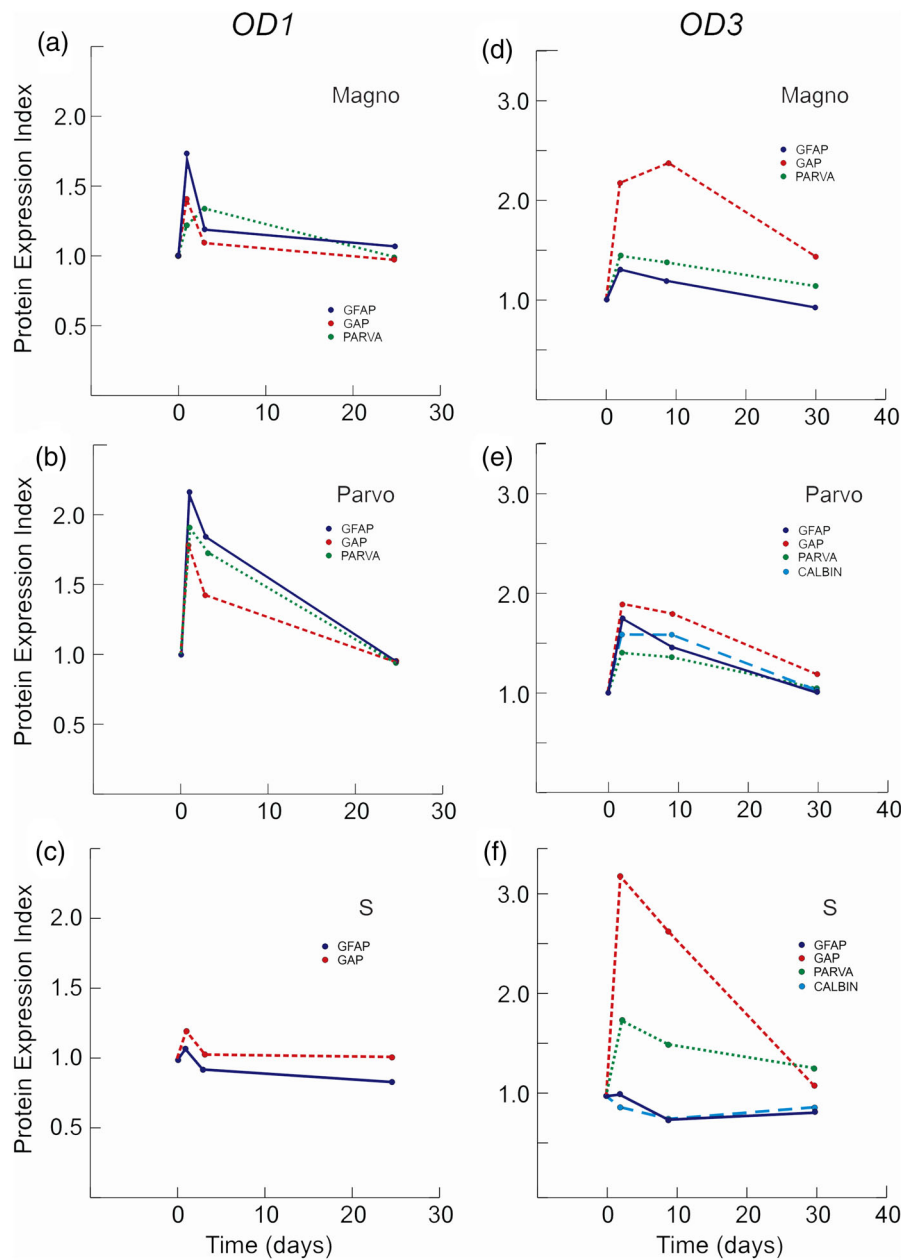


**FIGURE 8** Time course of the variation of protein expression index for GAP43, GFAP, calbindin, and parvalbumin in cases OD1 (left) and OD3 (right) for magnocellular (top), parvocellular (middle), and S (bottom) layers. Functions were drawn through the mean value of the data

that of GAP43. In the S layer, Cb expression varied little, with a slight increase observed in the first few days that returned to normal by the 30th day (Figure 7). ANOVA of the data obtained from OD3 only revealed a significant difference in the S layer ( $p = .019$ ).

### 3.5 | Expression of proteins

The data obtained for the expression of proteins showed substantial variability in different cases, probably related to the size and intensity of the lesion. In Case OD1, a substantial increase in GFAP expression was observed in the magnocellular layers (Figure 8a), while in Case

OD3 (Figure 8d), a larger increase was observed in GAP43 expression. The expression of both proteins decreased at 30th days after lesions were generated. The decrease in GFAP expression was more abrupt in Case OD1. The expression of Pv was similar in both cases.

The expression of these proteins in the parvocellular layers was similar in both cases (Figure 8b and 8e). Their levels increased after the lesion was induced and decreased to normal levels within 30 days. The expression of GAP43 exhibited the same pattern as that of GFAP, but GAP43 was expressed at lower levels in Case OD1 and higher levels in Case OD3.

The increase in GFAP and GAP43 expression in the S layer was smaller and not significant in Case OD1, but we observed a significant

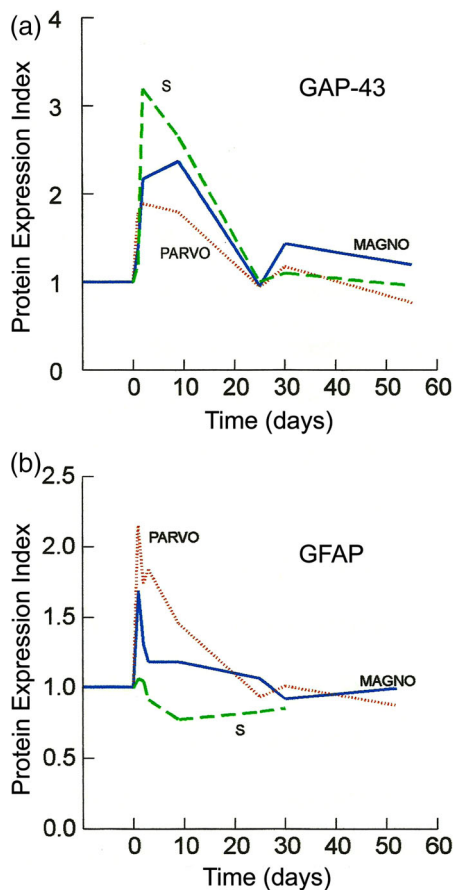


**FIGURE 9** Time course of the variation of the protein expression index of GAP43 (a) and GFAP (b) for magno-, parvocellular, and S layers. Functions were drawn through the mean value of the data

increase in GAP43 and Pv expression in Case OD3 (Figure 8c and 8f). The PEI curves for Case OD3 showed a distinct increase in the expression of GAP43 compared to the other proteins in the magnocellular and S layers, where a high level of synaptogenesis occurred (Figure 8c and 8f).

The analysis of the combined data from Cases OD1 and OD3 (Figure 9) revealed higher expression of GAP43 (synaptogenesis) in the S layer, followed by the magnocellular and parvocellular layers (Figure 9a). In addition, higher GFAP expression was detected in the parvocellular layer, followed by a transient increase in the magnocellular layer of the dLGN (Figure 9b). Therefore, GAP43 expression appeared to be increased in all layers after lesion induction, while the “cleansing” of the glial-damaged region (GFAP) is markedly greater in the parvocellular layers, followed by the magnocellular layer.

#### 4 | DISCUSSION

Here, we describe an increase or decrease in the expression of GFAP, GAP43, Cb, and Pv in all layers of the dLGN shortly after the lesion to the OD that returns to the original level with different time courses. Synaptogenesis (as evidenced by GAP43 expression) appears to be

increased in all layers, while “cleansing” of the glial-damaged region (GFAP) is markedly increased in the parvocellular layers, followed by the magnocellular layers.

By damaging the retinal fibers of ganglion cells, we trigger a process that will lead to a lesion of the dLGN neurons and a subsequent lesion of V1 neurons, as revealed here by the appearance of ocular dominance columns in layer IVc in this area. Since this process evolves over time, we generated laser-induced lesions at different time points and in different areas of the optic nerve disc to better study this process. We noted that the changes in V1 are perceived earlier than those in dLGN. The appearance of the ocular dominance columns in V1 is easily observed within 1 day of injury, whereas the effects on dLGN appear after a few days using the methods described here.

Pv, Cb, and calretinin are markers of distinct pathways involved in the development of the monkey dLGN (Yan et al., 1996). We subjected the dLGN sections to immunohistochemical staining to reveal the expression of proteins involved in the regeneration and functional modulation (GAP43) of synapses (Neve et al., 1988), proteins that facilitate the removal and restoration of the damaged glial tissue (GFAP) (Baekelandt et al., 1994), and the CaBPs Cb, and Pv, which function as secondary messengers and markers of certain types of neurons (Yücel et al., 2000).

Histograms of the densitometry analysis show a temporary increase in the expression of all proteins examined using immunohistochemistry. In animal OD1, the highest expression of GAP43 was detected in the parvocellular layers, as previously described in the literature (Baekelandt et al., 1994). In monkey OD3, where we intended to induce less pronounced lesions, the highest expression of GAP43 occurred in the magnocellular layers. This change in the pattern of plasticity prompted the question: Which layers are the first to be damaged and, consequently, does plastically respond differently to subacute damage? By observing the histograms depicting the expression of GFAP, we observed an increase in the expression of the protein within 1 day of lesion induction in all animals. This observation differs from reports in the literature that GFAP expression only increases beginning on the seventh day after injury, becomes very clear after 3 weeks, and persists for up to 7 weeks after the injury (Baekelandt et al., 1994; Leal et al., 1997). We cannot explain why we detected an increase in the expression of this protein within 1 day of injury in Case OD1. ANOVA only showed a significant change in the parvocellular layers for the combined samples from Cases OD1 and OD3.

ANOVA showed a significant difference in Pv staining preferentially in the parvocellular layers. According to Tigges and Tigges (1991), the immunoreaction for Pv in the dLGN labels small, medium, and large neurons in the magnocellular and parvocellular layers, as well as neurons of the interlayer and the S layer. In the control animal, Case OD4, Pv expression maintained this pattern in the S layer.

The magnitude of plastic changes induced by unilateral lesions at the border of the OD was reduced by the joint assessment of the ipsilateral and contralateral layers of the dLGN, poorly segregated in the capuchin monkey (Soares et al., 2001) and made it difficult to subjectively assess these changes in the photomicrographs of the nucleus. The use of an animal model with well-segregated layers, such

as the macaque to study these changes will allow an easy subjective assessment of plastic changes and the observation of these effects in reacted sections with the immunohistochemical methods used in this study.

The laser system used here enabled us to target select types of nerve fibers for disruption or damage. In the case of glaucoma, the choice of nerve fiber to disrupt is unpredictable, although the consensus is that the nerve fibers located in the upper and lower borders of the OD are the earliest to be affected by increased eye pressure (Glovinsky et al., 1993; Quigley et al., 1987). However, a consensus has not been reached on the nerve fibers located in the nasal and temporal quadrants. According to Dandona et al. (1991), temporal nerve fibers are affected to a greater extent than nasal fibers, considering the same eccentricity. The nasal fibers of the peripheral retina are relatively spared even in monkeys in which the optic nerve severely compromised by chronic glaucoma. In the study by Yücel et al. (2000), the difference between fiber losses in the nasal and temporal quadrants in an experimental glaucoma model was not statistically significant.

Few studies have examined the repercussion of glaucomatous lesions in the dLGN, and their conclusions are far from unanimous. Some authors have argued that the proportion of lesioned cells in the magnocellular layers of the dLGN is greater than that in the parvocellular layers, prompting the hypothesis that a chronic elevation of ocular pressure would cause selective damage in the magnocellular pathway (Dandona et al., 1991). The same conclusion was reported by Chaturvedi et al. (1993) based on the analysis of the dLGN in necropsy samples of the brains of humans with glaucoma compared to the dLGN of necropsied individuals without glaucoma. Weber et al. (2000) identified an equilibrium in the percentage of cells affected in the LGN of an experimental glaucoma model, and the percentages of cells in both the magnocellular and parvocellular layers were equally affected by a chronic elevation of ocular pressure. Other authors (Yücel et al., 2000) have reached the same conclusion as Weber et al. (2000), suggesting that recently developed and accurate methodology allows us to verify the balance between magnocellular and parvocellular neuronal or fiber loss in an experimental glaucoma model.

In contrast to the findings reported in this manuscript, Baekelandt et al. (1994) showed more pronounced increases in GAP43 expression in the S and interlaminar layers. We observed prominent changes in the parvocellular and magnocellular layers. In some cases, a higher concentration of the protein was detected in the central part of the nucleus than in the periphery of the magnocellular layer.

Farias et al. (2019) showed that lesions generated at different points of the retina caused different changes in dLGN and V1. In addition, ANOVA showed significant differences in the parvocellular layers but not in the magnocellular or S layers. This difference may be related to the fact that the absolute number of parvocellular cells is much larger than the number of magnocellular cells or koniocellular S cells. Dandona et al. (1991) subjected monkey brains to autoradiography to determine the effect of ocular pressure on the rapid phase of axonal transport. They found that an acute elevation of ocular pressure in four animals resulted in a decrease in the number of labeled cells in the

dLGN of two monkeys, a decrease in labeled cells in a third animal, and, finally, in the fourth monkey, they only observed a decrease in labeling in the parvocellular layer. This variation prompted us to speculate that the intensity of the laser-induced lesions in the OD may exert a similar effect on the dLGN and visual cortex in both subjects with acute glaucoma and chronic glaucoma.

Based on the experimental data, induced retinal lesions in monkeys or cats decrease afferents of cells in the primary visual cortex and induce a decrease in neuronal activity that may recover over time. The centers of the receptive fields of these cells are displaced toward healthy portions of the retina bordering the lesion (Baekelandt et al., 1996). Similar effects are observed in dLGN, although the extent of RF displacements in this nucleus is more modest than that in the cortex.

Studies of laser-induced retinal lesions have shown the neurons of V1 that originally represented the central area of the lesion become unresponsive to visual stimuli hours after lesion establishment (Darian-Smith & Gilbert, 1994; Gilbert & Wiesel, 1992). However, after days or months, the responsiveness of these cells recovers. In cats that suffered laser-induced lesions in the retina and then had the other eye enucleated, electrophysiological recordings 2–6 months after enucleation showed retinotopic reorganization of V1 (Kaas et al., 1990).

Similarly, monkeys that received bilateral retinal lesions showed a silent zone in V1 immediately after the lesions were generated. However, 75 days after the lesions were established, half of the cells recorded in the deprived areas of V1 recovered their responsiveness (Heinen & Skavenski, 1991). However, a study of the early stages of cortical reorganization of V1 showed that the recovery of cellular responses and visual topography occurs 6 h after the lesion (Botelho et al., 2014). We expect that similar changes should occur in dLGN, although we still need to address this question experimentally.

In the primary sensory cortex, a decrease in the mean evoked firing rate of Pv-positive inhibitory neurons is causally linked to a reorganization of excitatory networks following sensory perturbation (Feese et al., 2018). The authors suggest that Pv neurons are plastic in adults, raising the possibility that aspects of Pv response properties may be plastic throughout life (Feese et al., 2018). Takahata et al. (2018) examined the histochemical changes in the dLGN and the striate cortex (V1) in macaques. In the dLGN, neuronal atrophy and a dramatic increase in GFAP expression were observed in the lesion projection zones (Takahata et al., 2018).

An understanding of postlesion plasticity is critical to devise effective pharmacological and rehabilitative treatments. The GABAergic system is an important modulator of neuronal plasticity that plays an important role in controlling “critical periods” during brain development. Alia et al. (2016) reported an important role for GABAergic inhibition in functional restoration following ischemia in the adult mouse forelimb motor cortex. They also observed a delayed decrease in the levels of several GABAergic markers that accompanied cortical reorganization (Alia et al., 2016). In addition, activation of astrocytes in perilesional neural tissue after brain injury is important for brain homeostasis. Clearly, astrocytes play a key role in brain remodeling after injury (Neves et al., 2018). Thus, the hyperactivation of astrocytes (Neves et al., 2018) and the inhibition of GABAergic activity

(Alia et al., 2016) in the region of the representation of the retinal lesion in dLGN, as evidenced by the increased expression of GFAP and CaBPs, are beneficial for cortical reorganization. Astrocytes modulate the ionic balance and the secretion of synaptogenesis-related factors, facilitating the remodeling of neuronal circuits and cortical reorganization. A decrease in GABAergic activity, on the other hand, facilitates an increase in the synaptic strength of the subthreshold connections and the formation of new connections by the growing axons.

Glaucomatous lesions destroy fibers of the OD and produce a profound loss of peripheral vision and impairment of depth perception. We regard our massive laser-induced lesion as simulating glaucoma disorder. Laser-induced lesions on the border of the OD cause lesions of retinal fibers different from those of glaucoma. Nevertheless, these lesions cause changes in the visual system that are basically the same as those induced by glaucoma, either with respect to the plasticity of neurons or to the expression of proteins involved in the injury-regeneration processes. Although this type of lesion does not serve as a paradigm for comparison with the lesions obtained in the retina, due to the chronic increase in ocular pressure, it is suitable to study dLGN plasticity. In the present, we performed immunohistochemical staining and showed that brain plasticity at least partially compensates for retinal lesions in adult animals. We hope to enhance this recovery by reestablishing connections between the retina and dLGN. We propose to promote neuronal regeneration of the optic nerve either by grafting or stimulating the regeneration of the ganglion cell axons that are still alive, as has been suggested by Quigley (1998). The discovery of this type of process would benefit not only patients with glaucoma but also all those who have suffered trauma, inflammation, and vascular or degenerative diseases of the optic nerve. However, we propose that more detailed studies of dLGN and the visual cortex in individuals with glaucoma are necessary.

#### ACKNOWLEDGMENTS

We wish to thank Edil Saturato da Silva Filho and Liliane Herringer Motta for their skillful technical assistance. This work was supported by Fundação Carlos Chagas Filho de Amparo à Pesquisa do Estado do Rio de Janeiro, Grant/Award Number: E-26/110.192/2013, E-26/110.905/2013; Financiadora de Estudos e Projetos, Grant/Award Number: 0354/16

#### CONFLICT OF INTEREST

We declare that there is no conflict of interest, either financial, personal, or other relationships with other people or organizations within 3 years of beginning the submitted work that could inappropriately influence the results or interpretation of the data of the article.

#### AUTHOR CONTRIBUTIONS

All authors had full access to all the data in the study and take responsibility for the integrity of the data and the accuracy of the data analysis. SSP and RG planned the experiments. SSP, EPB, MFF, and RG executed the experiments, and discussed the data. RG wrote the manuscript. SSP and RG prepared the illustrations. RG, EPB, and JMS reviewed the data and revised the manuscript.

#### DATA AVAILABILITY STATEMENT

Data have not been shared. Our web repository is under construction. Data are available upon request to the corresponding author. Text and figures are available as supplementary data.

#### PEER REVIEW

The peer review history for this article is available at <https://publons.com/publon/10.1002/cne.25337>.

#### ORCID

Ricardo Gattass  <https://orcid.org/0000-0002-0321-1490>

#### REFERENCES

- Alia, C., Spalletti, C., Lai, S., Panarese, A., Micera, S., & Caleo, M. (2016). Reducing GABAA-mediated inhibition improves forelimb motor function after local cortical stroke in mice. *Science Report*, 6, 37823–37837.
- Baekelandt, V., Arckens, L., Annaert, W., Eysel, U. T., Orban, G. A., & Vandesande, F. (1994). Alterations in GAP-43 and synapsin immunoreactivity provide evidence for synaptic reorganization in adult cat dorsal lateral geniculate nucleus following retinal lesions. *European Journal of Neuroscience*, 6, 754–765.
- Baekelandt, V., Eysel, U. T., Orban, G. A., & Vandesande, F. (1996). Long-term effects of retinal lesions on growth-associated protein 43 (GAP-43) expression in the visual system of adult cats. *Neuroscience Letter*, 208, 113–116.
- Barsante, C., & Diniz, A. V. (1997). Xenônio x Argon x Criptônio x Diode. In J. A. H. de Freitas & J. Provenzano (Eds.), *Laser in ophthalmology* (pp. 89–97). Rio de Janeiro.
- Botelho, E. P., Ceriatte, C., Soares, J. G. M., Gattass, R., & Fiorani, M. (2014). Quantification of early stages of cortical reorganization of the topographic map of V1 following retinal lesions in monkeys. *Cerebral Cortex*, 24, 1–16.
- Bozini, D. G. (1997). Physical principles of laser. In J. A. H. de Freitas & J. Provenzano (Eds.), *Laser in ophthalmology* (pp. 1–18). Rio de Janeiro.
- Casagrande, V. A. (1994). A third parallel visual pathway to primate area V1. *Trends of Neuroscience*, 17, 305–310.
- Celio, M. R. (1990). Calbindin D-28k and parvalbumin in the rat nervous system. *Neuroscience*, 35, 375–475.
- Chaturvedi, N., Hedley-Whyte, E. T., & Dreyer, E. B. (1993). Lateral geniculate nucleus in glaucoma. *American Journal of Ophthalmology*, 116, 182–188.
- Dandona, L., Hendrickson, A., & Quigley, H. A. (1991). Selective effects of experimental glaucoma on axonal transport by retinal ganglion cells to the dorsal lateral geniculate nucleus. *Investigative Ophthalmology & Visual Science*, 32, 1593–1599.
- Darian-Smith, C., & Gilbert, C. D. (1994). Axonal sprouting accompanies functional reorganization in adult cat striate cortex. *Nature*, 368, 737–740.
- Farias, M. F., Ungerleider, L. G., Pereira, S. S., Amorim, A. K. J., Soares, J. G. M., & Gattass, R. (2019). Time course of cytochrome oxidase blob plasticity in the primary visual cortex of adult monkeys after retinal laser lesions. *Journal Comparative Neurology*, 527, 600–613.
- Feese, B. D., Pafundo, D. E., Schmehl, M. N., & Kuhlman, S. J. (2018). Binocular deprivation induces both age-dependent and age-independent forms of plasticity in parvalbumin inhibitory neuron visual response properties. *Journal of Neurophysiology*, 119, 738–751.
- Gallyas, F. (1979). Light insensitive physical developers. *Stain Technology*, 54, 173–176.
- Gattass, R., Souza, A. P. B., & Rosa, M. G. P. (1987). Visual topography in V1 in the Cebus monkey. *Journal Comparative Neurology*, 259, 529–548.
- Gilbert, C. D., & Wiesel, T. N. (1992). Receptive field dynamics in adult primary visual cortex. *Nature*, 356, 150–152.

- Glovinsky, Y., Quigley, H. A., & Pease, M. E. (1993). Foveal ganglion cell loss is size dependent in experimental glaucoma. *Investigative Ophthalmology & Visual Science*, 34, 395–400.
- Goodchild, A. K., & Martin, P. R. (1998). The distribution of calcium-binding proteins in the lateral geniculate nucleus and visual cortex of a New World monkey, the marmoset, *Callithrix jacchus*. *Visual Neuroscience*, 15, 625–642.
- Harwerth, R. S., Carter-Dawson, L., Shen, F., Smith, E. L. 3rd, & Crawford, M. L. (1999). Ganglion cells losses underlying visual field defects from experimental glaucoma. *Investigative Ophthalmology & Visual Science*, 40, 2242–2250.
- Heinen, S. J., & Skavenski, A. A. (1991). Recovery of visual responses in foveal V1 neurons following bilateral foveal lesions in adult monkey. *Experimental Brain Research*, 83, 670–674.
- Hendry, S. H., & Jones, E. G. (1986). Reduction in number of immunostained GABAergic neurones in deprived-eye dominance columns of monkey area 17. *Nature*, 320, 750–753.
- Higo, N., Oishi, T., Yamashita, A., Matsuda, K., & Hayashi, M. (2000). Expression of GAP-43 and SCG10 mRNAs in lateral geniculate nucleus of normal and monocularly deprived macaque monkeys. *Journal of Neuroscience*, 20, 6030–6038.
- Hof, P. R., & Nimchinsky, E. A. (1992). Regional distribution of neurofilament and calcium-binding proteins in the cingulate cortex of the macaque monkey. *Cerebral Cortex*, 2, 456–467.
- Johnson, J. K., & Casagrande, V. A. (1995). Distribution of calcium-binding proteins within the parallel visual pathways of a primate (*Galago Crassicaudatus*). *Journal Comparative Neurology*, 356, 238–260.
- Jones, E. G., & Hendry, S. H. (1989). Differential calcium binding protein immunoreactivity distinguishes classes of relay neurons in monkey thalamic nuclei. *European Journal of Neuroscience*, 1, 222–246.
- Kaas, J. H., Krubitzer, L. A., Chino, Y. M., Langston, A. L., Polley, E. H., & Blair, N. (1990). Reorganization of retinotopic cortical maps in adult mammals after lesions of the retina. *Science*, 248, 229–231.
- Leal, R. B., Gonçalves, C. A., & Rodnight, R. (1997). Calcium-dependent phosphorylation of glial fibrillary acidic protein (GFAP) in the rat hippocampus: A comparison of the kinase/phosphatase balance in immature and mature slices using tryptic phosphopeptide mapping. *Brain Research, Developmental Brain Research*, 104, 1–10.
- Malpeli, J. G., & Baker, F. H. (1975). The representation of the visual field in the lateral geniculate nucleus of *Macaca mulatta*. *Journal Comparative Neurology*, 161, 569–594.
- Medeiros, H. A. G. (1997). *Lentes utilizadas em fotocoagulação em: Laser in ophthalmology*. J. A. H. de Freitas & J. Provenzano (Eds.) (pp. 103–109). Rio de Janeiro.
- Mize, R. R., Luo, Q., & Tigges, M. (1992). Monocular enucleation reduces immunoreactivity to the calcium-binding protein calbindin 28 kD in the rhesus monkey lateral geniculate nucleus. *Visual Neuroscience*, 9, 471–482.
- Neve, R. L., Finch, E. A., Bird, E. D., & Benowitz, L. I. (1988). Growth-associated protein GAP-43 is expressed selectively in associative regions of the adult human brain. *Proceedings of the National Academy of Science U.S.A.*, 85, 3638–3642.
- Neves, J. D., Mestriner, R. G., & Netto, C. A. (2018). Astrocytes in the cerebral cortex play a role in the spontaneous motor recovery following experimental striatal hemorrhage. *Neural Regeneration Research*, 13, 67–68.
- Quigley, H. A. (1998). Selectivity in glaucoma injury. *Archives of Ophthalmology*, 116, 396–398.
- Quigley, H. A., Sanchez, R. M., Dunkelberger, G. R., L'Hernault, N. L., & Baginski, T. A. (1987). Chronic glaucoma selectively damages large optic nerve fibers. *Investigative Ophthalmology & Visual Science*, 28, 913–920.
- Rosa, M. G. P., Gattass, R., & Fiorani, Jr. M. (1988). Complete pattern of ocular dominance stripes in V1 of a New World monkey, *Cebus apella*. *Experimental Brain Research*, 72, 645–648.
- Silvermann, M. S., & Tootell, R. G. H. (1987). Modified technique for cytochrome oxidase histochemistry: Increased staining intensity and compatibility with 2-deoxyglucose autoradiography. *Journal of Neuroscience Methods*, 19, 1–10.
- Skene, J. H. (1989). Axonal growth-associated proteins. *Annual Review of Neuroscience*, 12, 127–156.
- Soares, J. G. M., Botelho, E. P., & Gattass, R. (2001). Distribution of calbindin, parvalbumin and calretinin in the lateral geniculate nucleus and superior colliculus in *Cebus apella* monkeys. *Journal of Chemical Neuroanatomy*, 22, 139–146.
- Takahata, T., Patel, N. B., Balam, P., Chino, Y. M., & Kaas, J. H. (2018). Long-term histological changes in the macaque primary visual cortex and the lateral geniculate nucleus after monocular deprivation produced by early restricted retinal lesions and diffuser induced form deprivation. *Journal Comparative Neurology*, 526, 2955–2972.
- Tigges, M., & Tigges, J. (1991). Parvalbumin immunoreactivity of the lateral geniculate nucleus in adult rhesus monkeys after monocular eye enucleation. *Visual Neuroscience*, 6, 375–382.
- Weber, A. J., Chen, H., Hubbard, W. C., & Kaufman, P. L. (2000). Experimental glaucoma and cell size, density, and number in the primate lateral geniculate nucleus. *Investigative Ophthalmology & Visual Science*, 41, 1370–1379.
- Wong-Riley, M. T. T. (1979). Changes in the visual system of monocularly sutured or enucleated cats demonstrable with cytochrome oxidase histochemistry. *Brain Research*, 171, 11–28.
- Yan, Y. H., Winarto, A., Mansjoer, I., & Hendrickson, A. (1996). Parvalbumin, calbindin, and calretinin mark distinct pathways during development of monkey dorsal lateral geniculate nucleus. *Journal of Neurobiology*, 31, 189–209.
- Yücel, Y. H., Zhang, Q., Gupta, N., Kaufman, P. L., & Weinreb, R. N. (2000). Loss of neurons in magno-cellular and parvo-cellular layers of the lateral geniculate nucleus in glaucoma. *Archives of Ophthalmology*, 118, 378–384.

**How to cite this article:** Pereira, S. S., Botelho, E. P., Soares, J.

G. M., Farias, M. F., & Gattass, R. (2022). Time course of dorsolateral geniculate nucleus plasticity in adult monkeys with laser-induced retinal lesions. *Journal of Comparative Neurology*, 530, 2385–2401.

<https://doi.org/10.1002/cne.25337>